11876 J. Agric. Food Chem. 2010, 58, 11876–11882
DOI:10.1021/jf1028366

JOURNAL OF AGRICULTURAL AND FOOD CHEMISTRY
ARTICLE

β-Cyclodextrin and Caffeine Complexes with Natural Polyphenols from Olive and Olive Oils: NMR, Thermodynamic, and Molecular Modeling Studies

Antonio Rescifina,*,† Ugo Chiacchio,† Daniela Iannazzo,‡ Anna Piperno,‡ and Giovanni Romeo‡

†Dipartimento di Scienze Chimiche, Università di Catania, Viale Andrea Doria 6, 95125 Catania, Italy, and ‡Dipartimento Farmaco-Chimico, Università di Messina, Viale S. S. Annunziata, 98168 Messina, Italy

Complexes of β-cyclodextrin (β-CD) and caffeine (Caf) with biophenols present in olive and olive oil (tyrosol, hydroxytyrosol, homovanillic acid, 3,4-dihydroxyphenylacetic acid, and protocatechuic acid) were investigated by NMR spectroscopy and thermodynamical−molecular dynamic studies to verify the formation of supermolecular aggregates. The obtained results indicated that the investigated biophenols form inclusion complexes with β-CD in a molar ratio of 1:1 in aqueous solution having binding constant values from 10- to 40-fold bigger than those of the corresponding complexes with Caf. Then, β-CD preferentially encloses the biophenol molecule, decreasing its bitter taste and, at the same time, preserving it against chemical and physical decomposition reactions that occur during storage.

KEYWORDS: β-Cyclodextrin; caffeine; biophenols; supramolecular interaction; NMR; molecular dynamics

INTRODUCTION

Biophenols, either in the form of extracts or as pure compounds, have been shown to counteract the effects of pro-inflammatory stimuli on target molecules (i.e., adhesion molecules) in different cell types, including cells of the arterial wall (*1*, *2*). Furthermore, biophenols play an important protective role against reactive oxygen species-induced oxidative injury in red blood cells (*3*), are involved in the synthesis of thromboxane in human cells, have been associated with a low incidence of cardiovascular diseases and cancer, inhibit phospholipid oxidation (*4*) and platelet-activating factor activity (*5*), and enhance nitric oxide production by mouse macrophages (*6*). In particular, olive biophenols (OBPs) contribute to the sensory and nutritional aspects of fresh and processed foods derived from *Olea europaea* (OE), representing test substrates in the sensorial perception and interesting antioxidant/chelating agents. The most biologically important OBPs, which are present as microcomponents in OE, are oleuropein, hydroxytyrosol, quercetin, ferulic acid, caffeic acid, *p*-hydroxyphenylacetic acid, *p*-coumaric acid, tyrosol, *p*-hydroxybenzoic acid, protocatechuic acid, 3,4-dihydroxyphenylacetic acid, homovanillic acid, and vanilethanediol (*7*).

Due to the importance of OE products in human health and in the Mediterranean diet, many studies have been developed to preserve OBPs against oxidation, especially during storage, and to mask or reduce their bitter taste to improve the palatability (*8*).

The activity of OBPs as antioxidant agents and radical scavengers against the biological damage caused by free radicals (*9*) requires in fact that these compounds are preserved by the decomposition which occurs when exposed to oxygen, light, and heat. One of the possibilities to stabilize them is the formation of inclusion complexes with cyclodextrins (CDs), a process that can actually be considered as a molecular encapsulation.

The formation of inclusion complexes between OBPs and CDs is described in the literature (*7*, *10*, *11*), but limited information has been reported about the OBP structural effects that control the modality of their encapsulation by CDs. Furthermore, it is well-known that the addition of CDs can reduce the bitter taste of drugs and foods by the formation of inclusion complexes (*12*, *13*). However, structural features and conformational alterations of OBPs that modify taste can also occur by interaction of the hydroxyl and carboxylic polar groups with the external surface of the CD.

The complex process of the taste perception can be considered as a supramolecular dynamic interaction between the sensorial receptors, the proteic and glycidic material present in the oral cavity, and OBPs (*14*). The different sensorial response to the taste stimulus may depend on the dimension and molecular structure of the OBPs with a different supramolecular reactivity.

The supramolecular interaction of 3,4-dihydroxyphenylacetic acid (3,4-DHPA) with carbohydrate or protein models has been reported by exploiting biomimetic NMR experiments, using CD and caffeine (Caf) as mimetics of the glycidic and proteic materials present in the oral cavity (*10*). In this paper, we have extended our study to other relevant OBPs contained in OE (**Figure 1**), to evaluate the competition of CD and Caf in the supermolecule formation with OBPs, through the determination of the thermodynamic parameters that control the complexation of the different biophenols. With regard to the encapsulation agent, we have chosen β-CD, which possesses an internal cavity of ∼6.6 Å (*15*),

*Author to whom correspondence should be addressed (phone +39-095-7385014; fax +39-06-233208980; e-mail arescifina@unict.it).

 Published on Web 11/03/2010

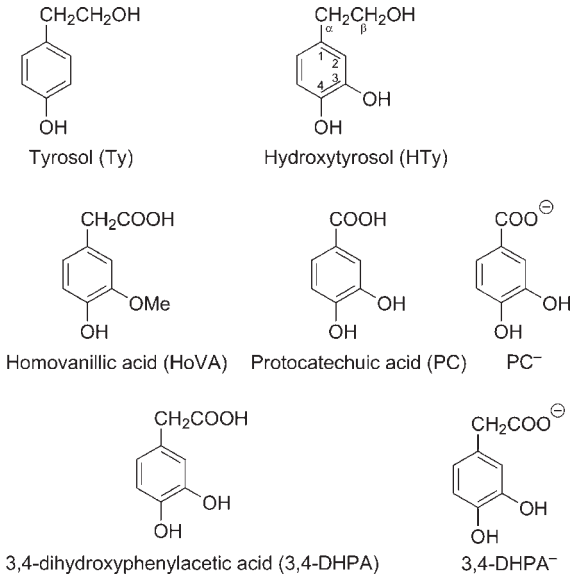

Figure 1. OBPs present in olive and olive oil and used for NMR experiments. The numeration of HTy, chosen as representative, is the one used for discussion.

compatible with the molecular shapes of the OBPs under investigation. Caf mimes the peptide linkage, being characterized by a molecular structure reminiscent of proline-rich peptides, particularly in the functionality $-CONMe_2$ for the presence of the carbonyl group and tertiary proline-like nitrogen atom. The obtained data could promote the comprehension of OBP interaction with human gustative buds and lead to the development of efficient technologies for preserving OBPs from oxidation and masking their bitter taste.

MATERIALS AND METHODS

Materials. β-CD, Caf, and OBPs were purchased from Aldrich (Milano, Italy); the sealed NMR tube with ethylene glycol was supplied by Varian (Torino, Italy). Before the measurements, OBPs and β-CD or Caf were mixed and equilibrated at the appropriate temperature for 10 min.

NMR Measurements. The ^1H and ^{13}C NMR spectra of the single molecules and their complexes were recorded in a Varian Unity Inova spectrometer, equipped with a 5 mm $^1H\{^{15}N-^{31}P\}$ PFG Indirect•nmr probe, at frequencies of 499.883 MHz (^1H) and 125.707 MHz (^{13}C) and at three different temperatures. All of the experiments were performed in a 99.96% D_2O solution (0.05 M for Caf and 0.002 M for β-CD) containing 0.03% of sodium 2,2-dimethyl-2-silapentane-5-sulfonate (DSS) as internal standard. In a typical experiment, 0.5 mL of Caf or β-CD solution was added with increasing amounts of 0.5 M solution of OBP to cover a concentration ratio OBP/Caf or OBP/β-CD varying from 1:1 to 60:1. The determination of the stoichiometry was accomplished by preparing equimolar solutions (20 mM) of β-CD and OBP species and mixing them to a constant volume of 0.5 mL, varying the desired ratio from 0.1 to 0.9 in 0.1 steps. The phase-sensitive transverse rotating-frame Overhauser effect spectroscopy (T-ROESY) experiments were run with a spectral width of 4000 Hz in 2K data points using 48 scans for each of the 512 t_1 increments and with HDO suppression. The spin lock time was set to 300 ms, and a field strength of 2 kHz was used. The data matrix was zero-filled to 4K × 2K, and a shifted square sinebell function was applied for processing in both dimensions. In all 2D experiments, 20 mM solutions of β-CD/OBP with a 1:1 molar ratio were used. ROEs were first converted to distance restraints using the vicinal $H_{5'}-H_{6'}$ proton cross-peak as calibration volume and an r^{-6} distance dependence function. Because intensities are influenced by fast-exchange regimen, data were interpreted in a semiquantitative way, classifying the Overhauser effects as strong (2.0−3.0 Å), medium (3.0−4.0 Å), or weak (4.0−5.0 Å). Selective nuclear Overhauser effect spectroscopy (1D NOESY) experiments, for OBP−Caf complexes, were performed using a 30 ms Gaussian-shaped selective pulse and a 1200 ms mixing time; other parameters were the same as those of 1D proton spectra. All of the spectra were acquired at three temperatures: 25, 40, and 60 °C. Temperature was controlled to ±0.1 °C with the control unit calibrated with a 100% ethylene glycol standard sample.

Computational Details. The initial geometries of OBP molecules were manually constructed and optimized at the PM3 level of theory. The starting β-CD structure for the simulation was extracted from the 1DMB entry of the RCSB PDB database (http://www.pdb.org). The CHARMM 27 force field was used, whereas the partial atomic charges were calculated by the Gasteiger method. Then, 562 TIP3P water molecules were added to a box with unit cell dimension $a = b = 29$ Å and $c = 22$ Å. In the simulation, all of the atoms and water molecules are free to move, and all atoms are treated explicitly. Periodic boundary conditions were adopted, and a cutoff radius of 11 Å was applied to the nonbonded interactions. The Ewald summation method was employed to evaluate the Coulombic interactions with a dielectric constant value of 1. The conformational search was carried out using a combined molecular mechanics−molecular dynamics simulated annealing protocol. According, β-CD structures were subjected to a simulated annealing process from 0 to 1000 K and back, performing iterations until the minimum energy conformation was found. The inclusion complexes were constructed from separately optimized β-CD and OBP geometries; these last were manually docked in the β-CD cavity, according to NMR observations, to obtain a good starting geometry for the complex, and then a simulation was carried out using a simulated annealing protocol (*16*): cooling from 300 to 50 K in 50 K steps, 15 ps simulation for each step, 1 fs time step, and energy minimization at the end of each step.

Mathematical Treatments. The equations and the methodologies used for the calculation of the association constants K_s and for the evaluation of thermodynamic parameters ΔH and ΔS are the same as previously reported and explained by us (*10*).

RESULTS AND DISCUSSION

OBP−β-CD Interaction. The inclusion geometry of OBPs in β-CD was investigated by ^1H NMR, ^{13}C NMR, T-ROESY, and molecular dynamics studies.

^1H NMR Studies. The insertion of OBP, as guest molecule into the hydrophobic cavity of β-CD, gives the opportunity to investigate the binding mechanism in aqueous solution and to elucidate the energies and geometries of the supramolecular complexes formed. Titration of OBPs with β-CD, carried out in D_2O solution, was performed by monitoring the modification of NMR frequencies of the signals of both partners.

The host−guest stoichiometry was established by using the continuous variation plot method (*17*). In the supramolecular formation, the resonances of β-CD H_3 and H_5 protons experienced the highest upfield shift, due to the OBP aromatic anisotropy, whereas H_2, H_4, and H_6 protons are almost unaffected (*18*). In all of the cases, the Job plots show a maximum at a molar ratio of 0.5 and highly symmetrical shapes, indicating that the supermolecule has a 1:1 stoichiometry and that no other supramolecular species are present. As an example, **Figure 2** reports the H_3 and H_5 proton shifts of HTy and PC after their inclusion in β-CD.

NMR experiments, carried out at three different temperatures, allowed the determination of the binding constants and the thermodynamic ΔH and ΔS parameters of the different OBPs. The results, reported in **Table 1**, show that PC has a tight fit toward the β-CD cavity, whereas HoVA has a loose interaction due to the steric hindrance exerted by the methyl group at C_3. Thus, with the exception of HoVA, all OBPs under study form a strong supramolecular complex with β-CD.

We have also investigated the binding constant for the inclusion of carboxylate anions of 3,4-DHPA and PC, respectively, at 25 °C (**Table 1**). The obtained data show that K_s values decrease going from the acid to its carboxylate anion, as previously reported for similar compounds (*19*).

^{13}C NMR Studies. ^{13}C NMR spectra of D_2O solutions containing OBP and β-CD consist of the resonances corresponding to

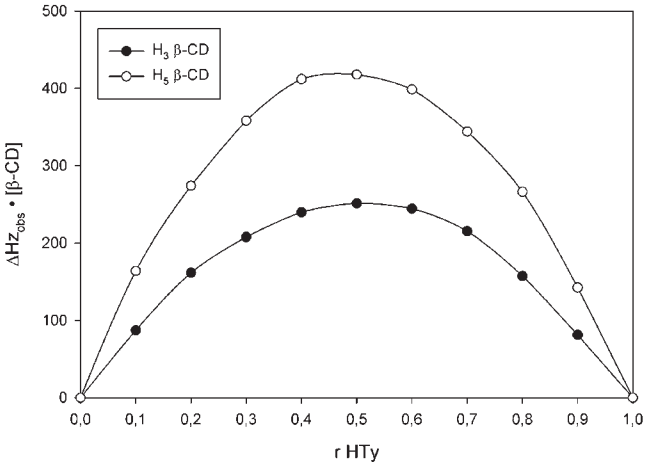

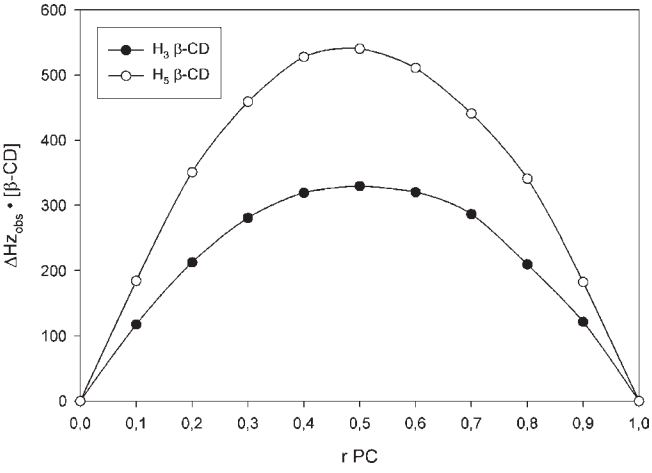

Figure 2. Job plots for HTy (left) and PC (right).

Table 1. Thermodynamic Parameters for the OBP−β-CD Supermolecules[a]

entry	OBP	$K_{25\,°C}$	$K_{40\,°C}$	$K_{60\,°C}$	$\Delta G_{25\,°C}$	$\Delta G_{40\,°C}$	$\Delta G_{60\,°C}$	ΔH	ΔS
1	Ty	497	318	179	−15.3	−14.9	−14.3	−24.1	−29.5
2	HTy	355	260	116	−14.6	−14.5	−13.1	−26.7	−40.6
3	HoVA	137	110	97	−12.2	−12.2	−12.6	−7.9	14.4
4	3,4-DHPA[b]	528	358	188	−15.5	−15.3	−14.5	−24.2	−29.0
5	PC	661	463	411	−16.0	−15.9	−16.6	−11.0	16.7
6	3,4-DHPA$^-$	191							
7	PC$^-$	219							

[a] K = M^{-1}; ΔG = kJ/mol; ΔH = kJ/mol; ΔS = J/mol·deg. [b] Values have been taken from ref *10*.

Table 2. ^{13}C NMR Chemical Shift Displacements in the OBP−β-CD Supermolecules[a]

entry	OBP	$\Delta\delta_{C1}$	$\Delta\delta_{C4}$	$\Delta\delta_{C\alpha}$
1	Ty	−0.73	0.58	−0.99
2	HTy	−0.71	0.65	−1.09
3	HoVA	−1.15	1.01	−1.37
4	3,4-DHPA	−1.23	1.13	−1.43
5	PC	0.81	−1.32	1.49
6	3,4-DHPA$^-$	0.88	−0.98[b]	1.13
7	PC$^-$	1.89	−0.35	2.35

[a] Negative signs indicate upfield displacements. [b] C_3 is equally affected.

six nonequivalent β-CD carbon atoms and the expected number of signals due to the substrate species.

Previously reported ^{13}C NMR studies of α-CD inclusion complexes with substituted aromatic guests in aqueous solution have shown that the included head carbons are largely shielded, whereas the corresponding tail carbons show a large deshielding (*20*). The fact that some aromatic compounds, upon inclusion in CDs in aqueous solution, show UV spectral changes almost identical with that observed when the compounds are moved from aqueous to dioxane solution strongly suggests that the ^{13}C shift changes of the substituted aromatic guests should arise from the change in environment from a highly polar (water, with dielectric constant ε = 78.3) to a more apolar one (dioxane, with ε = 2) (*21*).

The results of our experiments with β-CD are summarized in **Table 2**. Entries 1−4 indicate a penetration of the head (the C_1 side) of OBP from the secondary hydroxyl site of β-CD, whereas from the examination of entries 5−7 it is evident that PC, its anion, and the anion of 3,4-DHPA penetrate always from the secondary rim with an inverted orientation, that is, with the carboxylic moiety, the tail, directed toward the external environment.

In fact, the first type of orientation is supported by the shielding of included C_1 and Cα carbons ($\Delta\delta_{C1}$ and $\Delta\delta_{C\alpha}$) compared with deshielding of corresponding para carbons ($\Delta\delta_{C4}$). Whereas for PC, PC$^-$, and 3,4-DHPA$^-$ the observed shifts point out that the insertion in β-CD occurs from the tail, the values of C_4 displacements are in accordance with the picture above delineated.

T-ROESY Studies. The orientation above determined is fully confirmed by T-ROESY NMR experiments. In fact, in the T-ROESY spectra of the OBP−β-CD systems cross-peaks connecting the β-CD H_3 and H_5 resonances to that of OBP protons can be observed (**Table 3**). In particular, for entries 1−4, it is evident that H_2, H_6, and H_α protons of OBP show the greatest NOE contact interaction, from strong to medium, with H_5 of β-CD and, contemporarily, the $H_{(3)5}$ of OBP show the maximum interaction with H_3 of β-CD, suggesting a deep inclusion by the head, with H_2 and H_6 protons placed almost in the middle with respect to β-CD H_3 and H_5. On the contrary, for entries 5−7, these interactions are inverted, thus indicating an insertion of OBPs by the tail. Moreover, in the case of PC$^-$ the values of the NOE contacts point out a moderate insertion.

Computational Studies. The supramolecular complexes of OBPs in β-CD have been investigated by molecular modeling methodology, to confirm and rationalize the observed inclusion geometry. In this aim, both head and tail inclusion orientations, from the β-CD secondary rim, were considered. The final relative stability energy values, referred to the more stable complex in each couple, of all optimized complexes in water, together with the respective Boltzmann distributions, are reported in **Table 4**. The optimized structures of the most stable complex for each of the four couples are represented in **Figure 3**. Once again, the results well agree with the experimental data, highlighting the structural outcome of the supramolecular aggregates. With the exception of the 3,4-DHPA anion, all OBPs insert into the β-CD cavity almost coaxially. In particular, 3,4-DHPA$^-$ is visibly inclined, with the C_3 and C_4 carbon atoms perpendicular to the β-CD cavity axis, principally because of the unsaturation of a hydrogen bond between 3-OH and an oxygen atom of the primary alcoholic moiety of β-CD. Another hydrogen bond is present in the PC complex, between the phenolic functionality and the anomeric oxygen: the interaction anchors the OBP coaxially.

The Boltzmann distributions underscore, for the 3,4-DHPA, the unsaturation of an equilibrium between the head and tail orientation insertion as observed for similar compounds (*22*). Finally, the inversion registered in the couple for 3,4-DHPA and

Table 3. Observed Intermolecular Cross-Peaks in the T-ROESY Spectra of OBP Complexes with the Protons Located Inside the β-CD Cavity[a]

entry	OBP protons	β-CD H_3	β-CD H_5
1	Ty		
	$H_{2,6}$	+++	+++
	$H_{3,5}$	++	+
	H_α	+	+++
	H_β	−	++
2	HTy		
	$H_{2,6}$	+++	++
	H_5	++	+
	H_α	+	++
	H_β	+	+++
3	HoVA		
	$H_{2,6}$	+++	++
	H_5	++	−
	H_α	++	++
4	3,4-DHPA		
	$H_{2,6}$	+++	+++
	H_5	++	+
	H_α	+	+++
5	PC		
	$H_{2,6}$	++	+
	H_5	+	++
6	3,4-DHPA$^-$		
	$H_{2,6}$	++	++
	H_5	++	+++
	H_α	++	+
7	PC$^-$		
	$H_{2,6}$	+	−
	H_5	++	+

[a] Relative intensity of the peaks: +++ = strong, ++ = medium, + = weak, − = no signal.

Table 4. Relative Stability Energies, Obtained by Molecular Dynamic Studies, between the Up- and Down-Oriented Couples of Selected OBPs and Their Boltzmann Distributions and Dipolar Moments

OBP	$\Delta\Delta E$[a]	Boltzmann distribution[b]	dipolar moment[c]
3,4-DHPA head	0.00	92.64	0.97[d]
3,4-DHPA tail	6.32	7.36	
PC head	39.47	0.00	0.92[e]
PC tail	0.00	100.00	
3,4-DHPA$^-$ head	10.63	1.39	12.67[e]
3,4-DHPA$^-$ tail	0.00	98.61	
PC$^-$ head	15.44	0.21	12.94[e]
PC$^-$ tail	0.00	99.79	

[a] $\Delta\Delta E$ = kJ/mol. [b] In percent. [c] For the isolated molecule, calculated at PM3 level in gas phase. [d] Directed toward the 4-hydroxylic moiety. [e] Directed toward the carboxylic moiety.

its anion is fully explainable considering the electronic effects. It is well-known that CDs have a large dipole moment which points from the wider rim toward the narrow one (*23*); thus, an antiparallel arrangement of the dipoles between host and guest molecules favors the binding. The dipole moments, reported in **Table 4**, account for the inversion registered by the 3,4-DHPA with respect to PC and the corresponding anions. In fact, the dipole moment of the 3,4-DHPA, pointing toward the C_4 atom, is inverted with respect its anion, where the dipole moment is directed toward C_1. For PC and its anion, the dipole moment is direct toward C_1 because of the conjugation of the carboxylic moiety with the aromatic ring.

Table 5. Thermodynamic Parameters for the OBP−Caf Supermolecules[a]

entry	OBP	$K_{25\,°C}$	$K_{40\,°C}$	$K_{60\,°C}$	$\Delta G_{25\,°C}$	$\Delta G_{40\,°C}$	$\Delta G_{60\,°C}$	ΔH	ΔS
1	Ty	4	3	2	−3.6	−2.5	−1.9	− 18.9	−51.3
2	HTy	9	7	5	−5.5	−5.2	−4.7	− 12.1	−22.1
3	HoVA	8	4	1	−5.1	−3.4	−1.0	− 39.9	−117.7
4	3,4-DHPA[b]	16	12	5	−6.9	−6.5	−4.4	− 28.4	−71.0
5	PC	57	49	19	−10.0	−9.5	−8.1	− 26.3	−54.7

[a] K = M^{-1}; ΔG = kJ/mol; ΔH = kJ/mol; ΔS = J/mol·deg. [b] Values have been taken from ref *10*.

OBP−Caf Interaction. The addition of OBPs to a solution of Caf in D_2O results in the modification of the NMR frequencies of the signals of both partners. As already reported (*10*), the Caf H_8 proton experienced the highest upfield shift, and its drifting was used to determine the binding constants. All experiments were performed at three different temperatures to provide the evaluation of thermodynamic ΔH and ΔS parameters.

The obtained association constants (K_s) are reported in **Table 5**, together with enthalpy and entropy values. PC shows the most favorable association constant. In particular, the presence of a second free hydroxylic functionality improves the supramolecular interaction (see entry 1 vs 2 and entry 3 vs 4). Moreover, the conjugation of the carboxylic with the aromatic nucleus (see entry 4 vs 5) increases to ≈3.5 times the value of K_s: this can be rationalized on the basis of the full planarity of PC with respect to 3,4-DHPA, leading to a better coplanarity of the formed supermolecule. Because the bitterness can be connected with the association intensity of OBP to the taste receptor, here represented by Caf, the obtained data suggest that PC possesses the greater bitter taste perception, followed by 3,4-DHPA, HTy, HoVA, and Ty. It has been reported that the threshold of bitterness perception for Ty is at a concentration of 10−14 mg/L (*24*); thus, it is expected that PC induces a bitter sensation with a threshold of about 1 mg/L.

In all cases, 1D NOESY experiments show a through-space interaction between the Caf N_3 and N_7 methyl groups with the aromatic protons of OBPs, with an average separation distance of ≈3.5 Å. These data indicate that the OBP−Caf supermolecules form a charge transfer, weakly π-bonded, molecular complex, the formation of which can be rationalized in terms of frontier molecular orbital (FMO) interactions. The values for the HOMO and LUMO of OBPs and Caf, obtained by semiempirical PM3 calculations, show that all of the OBPs approach the Caf molecule according to a HOMO−LUMO interaction, with the exception of PC in which the opposite LUMO−HOMO interaction prevails (**Figure 4**). The HOMO−LUMO energy gaps are completely in accord with the association constant values obtained at 60 °C, with some discrepancies with respect to the values at 25 °C. This behavior is probably imputable to a solvent effect that decreases with increasing temperature, thus approaching the calculation in vacuum, in accordance with the lowering of the dielectric constant that goes from ε = 78.3 to 66.7 (*25*).

Thermodynamic Considerations. The enthalpy and entropy values measured in water for OBP−β-CD and OBP−Caf supermolecules, all negatives with the exception of entropy values for β-CD−HoVA and β-CD−PC supermolecules, are indicative of the absence of a "classical" hydrophobic effect, characterized by $\Delta H \approx 0$ and $T\Delta S > 0$.

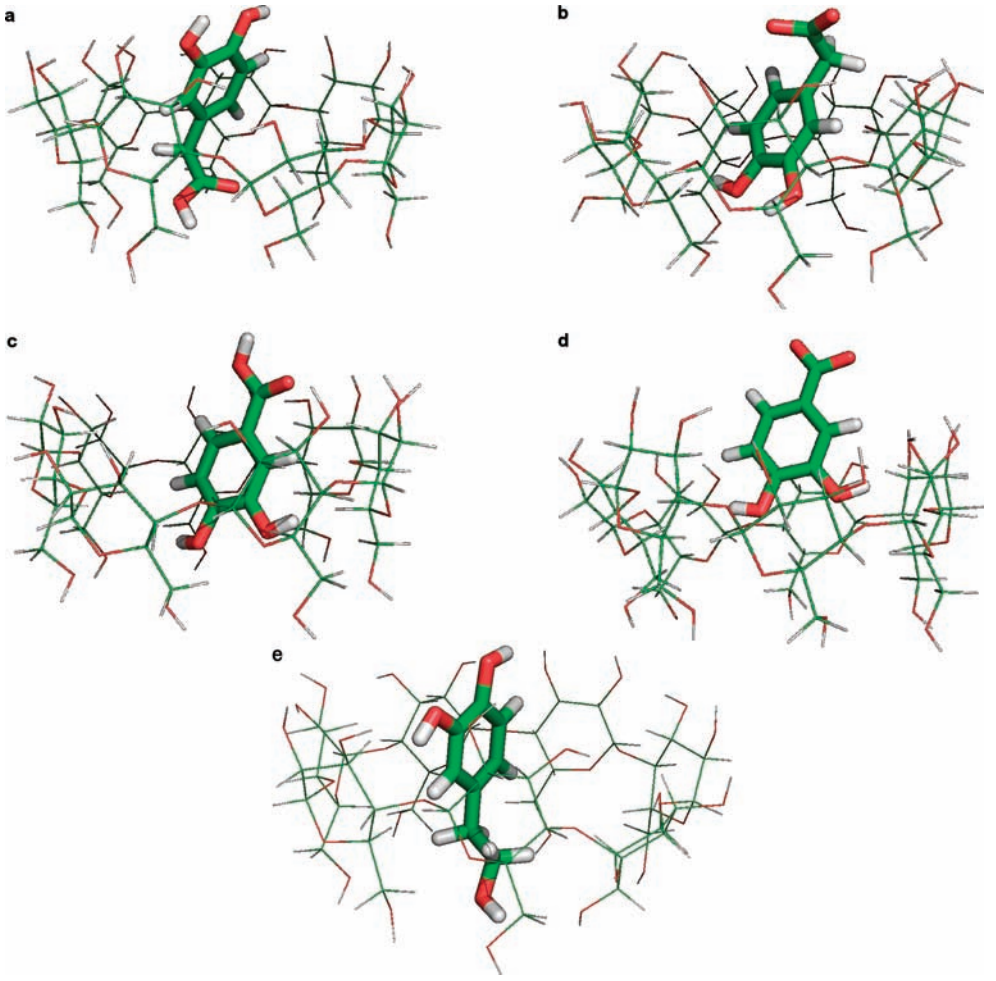

Figure 3. Most stable optimized structures of the β-CD complexes with (**a**) 3,4-DHPA in the up orientation, (**b**) 3,4-DHPA anion in the down orientation, (**c**) PC in the down orientation, (**d**) PC anion in the down orientation, and (**e**) HTy in the up orientation.

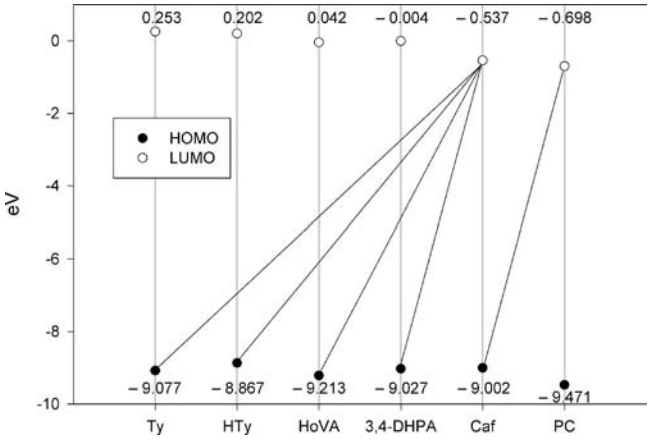

Figure 4. Calculated HOMO and LUMO energies for all OBPs and Caf molecules.

We have also ascertained the presence of an " enthalpy−entropy compensation" (*26*), a term utilized to describe the behavior of ΔH and ΔS for a series of similar reactions driven by changes in water solvation. This effect is characterized by a linear relationship between ΔH and ΔS, indicating that the resulting change in $T\Delta S$ is proportional to the accompanying change in ΔH. In processes such as a supermolecule formation, where changes in the solvation of both guest and host play a fundamental role in determining the stability of the supermolecules (*27*), this effect can give important information. The plots of the entropy changes ($T\Delta S$) against the enthalpy changes (ΔH), on the basis of the equation $T\Delta S = \alpha\Delta H + T\Delta S_0$, are reported in **Figure 5** for OBP−Caf and OBP−β-CD complexes. The α slope is a quantitative measure of the entropic canceling of the enthalpic gain from the supramolecular formation. In other words, only a proportion $(1 - \alpha)$ of the increment in ΔH contributes toward the raising of the supermolecule stability ($-\Delta G$). Moreover, as far as the intercept ($T\Delta S_0$) is positive, the supermolecule formation can take place even in the absence of an enthalpic gain. This situation is quite likely to occur when the entropic contribution from the desolvation process is the major factor governing the supermolecule formation. Thus, the slope and the intercept of the $\Delta H - T\Delta S$ plot are characteristic of the ligand topology and the supermolecule stoichiometry and can be used as a quantitative measure of ligand conformational change and of the extent of ligand desolvation caused by the supermolecule formation (*28*).

From this consideration and from the α and $T\Delta S_0$ values obtained for OBP−Caf ($\alpha = 0.97$, $T\Delta S_0 = 5.51$ kJ/mol, $r^2 = 0.95$) and OBP−β-CD supermolecules ($\alpha = 0.92$, $T\Delta S_0 = 13.19$ kJ/mol, $r^2 = 0.97$) under study (**Figure 5a**), it is possible to conclude that, despite the apparently rigid skeletons of OBPs, Caf, and β-CD, the supramolecular event causes substantial conformational changes also involving the reorganization of the original hydrogen bond network, whereas the intercepts of 5.5 and 13.2 indicate that an extensive dehydration occur upon interaction of OBPs with both Caf and β-CD. The higher intrinsic entropic gain ($\Delta H_0 = 0$), achieved for OBP−β-CD complexes, is imputable to the additional

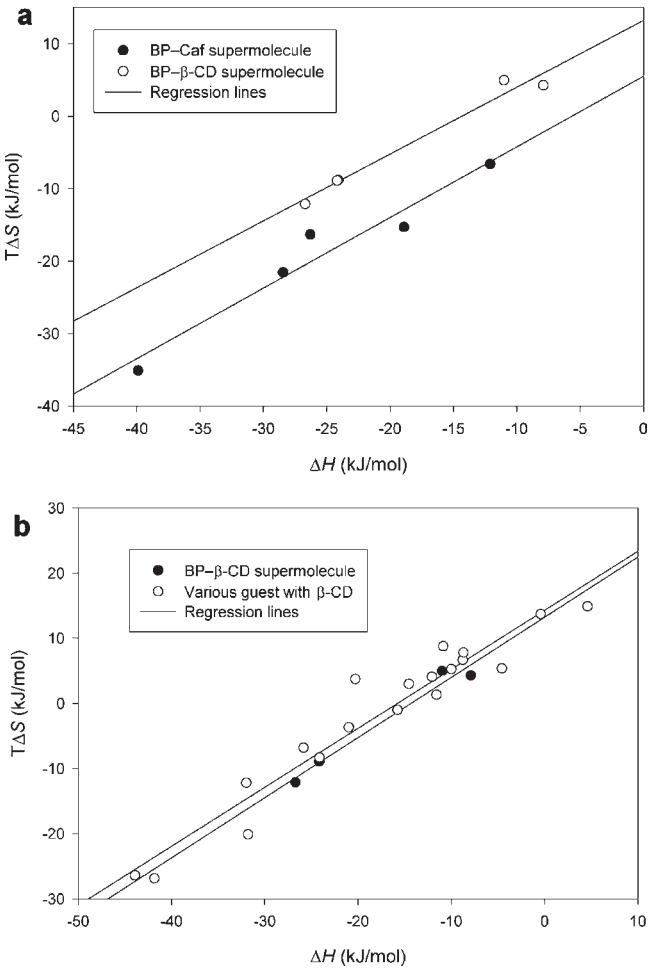

Figure 5. Linear regression plots of the entropy changes against the enthalpy changes for (**a**) the OBP−Caf and OBP−β-CD supermolecules under study and (**b**) the OBP−β-CD supermolecules under study compared with other experimental literature data for similar inclusion compounds.

release of water molecules that were originally residing within the cavity and to the induced dehydration from the peripheral hydroxyl groups of cyclodextrin.

Figure 5b reports a comparison of the values obtained for OBP−β-CD supermolecules against other similar inclusion compounds with β-CD, reported in the literature (*29*). It is evident that our values are in accordance with this type of supramolecular species (α = 0.90, $T\Delta S_0$ = 14.29 kJ/mol, r^2 = 0.93).

Moreover, inspection of **Table 2** shows that with the increase of the temperature, the magnitude of the apparent stability constant of the OBP−β-CD complex decreases. This behavior is typical of an exothermic and enthalpy-driven process ($|\Delta H| > T|\Delta S|$), as usually found for associations between small guest molecules and an apolar cavity in water. The effect can be ascribed to a possible reduction of OBP/β-CD interaction forces, such as van der Waals and hydrophobic forces (*30*). The same considerations are valid for the stability constants of OBP−Caf complexes reported in **Table 5**.

In some cases, however, temperature changes may have a negligible effect when the guest/CD interaction is predominantly entropy driven (*31*); this effect begins to be perceptible for entries 3 and 5 of **Table 2**, which have a positive enthalpic value, where the change from 40 to 60 °C leads only to a small change in K_s.

In conclusion, the NMR spectroscopic and thermodynamical−molecular dynamic studies indicate that all of the investigated OBPs form inclusion complexes with β-cyclodextrin in a molar ratio of 1:1, in aqueous solution, with binding constant values from 10- to 40-fold higher than that of the corresponding complexes with Caf. Thus, β-CD can preferentially enclose the OBP molecule, thus decreasing its bitter taste and, at the same time, preserving it against chemical and physical decomposition reactions that operate during storage.

Moreover, if the bitterness degree can effectively be reproduced by the association constant value of OBP with β-CD and caffeine, this method could be used to construct a new type of scale to measure the relative bitterness of compounds.

ACKNOWLEDGMENT

We are grateful to Prof. Nicola Uccella for his helpful advice and fruitful discussions.

LITERATURE CITED

(1) Dell'Agli, M.; Fagnani, R.; Galli, G. V.; Maschi, O.; Gilardi, F.; Bellosta, S.; Crestani, M.; Bosisio, E.; De Fabiani, E.; Caruso, D. Olive oil phenols modulate the expression of metalloprotinase 9 in THP-1 cells by acting on nuclear factor-κB signaling. *J. Agric. Food Chem.* **2010**, *58*, 2246−2252.

(2) Miles, E. A.; Zoubouli, P.; Calder, P. C.; Phil, D. Differential anti-inflammatory effects of phenolic compounds from extra virgin olive oil identified in human whole blood cultures. *Nutrition* **2005**, *21*, 389−394.

(3) Paiva-Martins, F.; Fernandes, J.; Santos, V.; Silva, L.; Borges, F.; Rocha, S.; Belo, L.; Santos-Silva, A. Powerful protective role of 3,4-dihydroxyphenylethanol-elenolic acid dialdehyde against erythrocyte oxidative-induced hemolysis. *J. Agric. Food Chem.* **2010**, *58*, 135−140.

(4) Soler-Rivas, C.; Espín, J. C.; Wichers, H. J. Oleuropein and related compounds. *J. Sci. Food Agric.* **2000**, *80*, 1013−1023.

(5) Andrikopoulos, N. K.; Antonopoulou, S.; Kaliora, A. C. Oleuropein inhibits LDL oxidation induced by cooking oil frying by-products and platelet aggregation induced by platelet-activating factor. *Lebensm. Wiss. Technol.* **2002**, *35*, 479−484.

(6) Visioli, F.; Bellosta, S.; Galli, C. Oleuropein, the bitter principles of olives, enhances nitric oxide production by mouse macrophages. *Life Sci.* **1998**, *62*, 541−546.

(7) Mourtzinos, I.; Salta, F.; Yannakopoulou, K.; Chiou, A.; Karathanos, V. T. Encapsulation of olive leaf extract in β-cyclodextrin. *J. Agric. Food Chem.* **2007**, *5*, 8088−8094.

(8) Baiano, A.; Terracone, C.; Gambacorta, G.; La Notte, E. Changes in quality indices, phenolic content and antioxidant activity of flavored olive oils during storage. *J. Am. Oil Chem. Soc.* **2009**, *86*, 1083−1092.

(9) Ouyang, Y.-Z.; Ma, C.-J.; Yu, J.; Huang, Q. Study on the stabilization of anti-photosensitivity and ultrasonic irradiation for vitamin E and its inclusion compound by β-cyclodextrin. *Shi-pin Ke-ji* (*Food Sci. Technol.*) **2006**, *31*, 62−65.

(10) Bianco, A.; Chiacchio, U.; Rescifina, A.; Romeo, G.; Uccella, N. Biomimetic supramolecular biophenol−carbohydrate and biophenol−protein models by NMR experiments. *J. Agric. Food Chem.* **1997**, *45*, 4281−4285.

(11) Efmorfopoulou, E.; Rodis, P. Complexation of oleuropein and *trans*-cinnamic acid with cyclodextrins. *Chem. Nat. Compd.* **2004**, *40*, 362−366.

(12) Martin Del Valle, E. M. Cyclodextrins and their uses: a review. *Process Biochem.* **2004**, *39*, 1033−1046.

(13) Szente, L.; Szejtli, J. Cyclodextrins as food ingredients. *Trends Food Sci. Technol.* **2004**, *15*, 137−142.

(14) Chaudhari, N.; Roper, S. D. The cell biology of taste. *J. Cell Biol.* **2010**, *190*, 285−296.

(15) Lichtenthaler, F. W.; Immel, S. Molecular modeling of saccharides. Part 9. On the hydrophobic characteristics of cyclodextrins: computer-aided visualization of molecular lipophilicity patterns. *Liebigs Ann. Chem.* **1996**, 27−37.

(16) Scheraga, H. A. Predicting three-dimensional structures of oligopeptides. In *Reviews in Computational Chemistry*; Lipkowitz, K. B., Boyd, D. B., Eds.; VCH: New York, 1992; Vol. 3, pp 73−142.

(17) Job, P. Formation and stability of inorganic complexes in solution. *Ann. Chim. Appl.* **1928**, *9*, 113−203.

(18) Ejchart, A.; Koźmiński, W. NMR of cyclodextrins and their complexes. In *Cyclodextrins and their Complexes: Chemistry, Analytical Methods, Applications*; Dodziuk, H., Ed.; Wiley-VCH Verlag: Weinheim, Germany, 2006; pp 231−254.

(19) Davies, D. M.; Savage, J. R. Cyclodextrin complexes of substituted perbenzoic and benzoic acids and their conjugate bases: free energy relationships show the interaction of polar and steric factors. *J. Chem. Soc., Perkin Trans. 2* **1994**, 1525−1530.

(20) Gelb, R. L.; Schwartz, L. M.; Cardelino, B.; Fuhrman, H. S.; Johnson, R. F.; Laufer, D. A. Binding mechanisms in cyclohexaamylose complexes. *J. Am. Chem. Soc*. **1981**, *103*, 1750−1757.

(21) Inoue, Y.; Hoshi, H.; Sakurai, M.; Chûjô, R. Geometry of cyclohexaamylose inclusion complexes with some substituted benzenes in aqueous solution based on carbon-13 NMR chemical shifts. *J. Am. Chem. Soc.* **1985**, *107*, 2319−2323.

(22) Liu, L.; Guo, Q.-X. Novel prediction fort he driving force and guest orientation in the complexation of α- and β-cyclodextrin with benzene derivatives. *J. Phys. Chem. B* **1999**, *103*, 3461−3467.

(23) Rekharsky, M. V.; Inoue, Y. Complexation thermodynamics of cyclodextrins. *Chem. Rev*. **1998**, *98*, 1875−1918.

(24) Andrade, P.; Seabra, R.; Ferreira, M.; Ferreres, F.; García-Viguera, C. Analysis of non-coloured phenolics in port wines by capillary zone electrophoresis: influence of grape variety and ageing. *Z. Lebensm. Unters. Forsch. A* **1998**, *206*, 161−164.

(25) Owen, B. B.; Miller, R. C.; Milner Harold, C. E.; Cogan, L. The dielectric constant of water as a function of temperature and pressure. *J. Phys. Chem*. **1961**, *65*, 2065−2070.

(26) Lumry, R.; Rajender, S. Enthalpy-entropy compensation phenomena in water solutions of proteins and small molecules: a ubiquitous properly of water. *Biopolymers* **1970**, *9*, 1125−1127.

(27) Clarke, R. J.; Coates, J. H.; Lincoln, S. F. Inclusion complexes of the cyclomalto-oligosaccharides (cyclodextrins). *Adv. Carbohydr. Chem. Biochem*. **1988**, *46*, 205−249.

(28) Rekharsky, M. V.; Inoue, Y. Complexation thermodynamics of cyclodextrins. *Chem. Rev*. **1998**, *98*, 1875−1918.

(29) Jencks, W. P. Hydrophobic forces. In *Catalysis in Chemistry and Enzymology*; Dover, Ed.; General Publishing: Toronto, Canada, 1987; p 427.

(30) Zarzycki, P. K.; Lamparczyk, H. The equilibrium constant of β-cyclodextrin−phenolphthalein complex; influence of temperature and tetrahydrofuran addition. *J. Pharm. Biomed. Anal*. **1998**, *18*, 165−179.

(31) Nagase, Y.; Hirata, M.; Wada, K.; Arima, H.; Hirayama, F.; Irie, T.; Kikuchi, M.; Uekama, K. Improvement of some pharmaceutical properties of DY-9760e by sulfobutyl ether β-cyclodextrin. *Int. J. Pharm*. **2001**, *229*, 163−172.

Received for review July 20, 2010. Revised manuscript received October 14, 2010. Accepted October 20, 2010. This work was partially supported by CINMPIS and MIUR (PRIN).